



Contents lists available at ScienceDirect

International Journal of Rock Mechanics and Mining Sciences

journal homepage: <http://www.elsevier.com/locate/ijrmms>

## Impact of rock fracture geometry on geotechnical barrier integrity – A numerical study

Florian M. Huber<sup>a,\*</sup>, Debora Leone<sup>a</sup>, Michael Trumm<sup>a</sup>, Luis R. Moreno<sup>b</sup>, Ivars Neretnieks<sup>b</sup>, Achim Wenka<sup>c</sup>, Thorsten Schäfer<sup>d</sup>

<sup>a</sup> Karlsruhe Institute of Technology (KIT), Institute for Nuclear Waste Disposal (INE), P.O. Box 3640, D-76021, Karlsruhe, Germany

<sup>b</sup> Department of Chemical Engineering and Technology, Royal Institute of Technology, Stockholm, Sweden

<sup>c</sup> Karlsruhe Institute of Technology (KIT), Institute for Micro Process Engineering (IMVT), Hermann-von-Helmholtz-Platz 1, DE-76344, Eggenstein-Leopoldshafen, Germany

<sup>d</sup> Friedrich-Schiller-University Jena (FSU), Institute of Geosciences, Applied Geology, Burgweg 11, 07749, Jena, Germany

### ARTICLE INFO

#### Keywords:

Radioactive waste disposal  
Multi-barrier systems  
Low-salinity groundwater  
Crystalline rock  
Rock fracture

### ABSTRACT

The effect of fracture geometry on bentonite erosion for a generic repository site in crystalline host rock environment was investigated by means of 2-d numerical simulations. Fracture geometry was varied systematically using random aperture normal distributions with a mean aperture of 1 mm and standard deviations between 0 and 0.7 mm, respectively. Moreover, two aperture correlation lengths (0.2 m and 2 m) were applied. Based on the synthetic fracture aperture fields generated the cubic law in conjunction with the Darcy equation is used to simulate fracture flow fields for mean flow velocities in the fracture between  $1 \times 10^{-5}$  m/s and  $1 \times 10^{-7}$  m/s. These flow fields are used in a two-way coupling approach to bentonite erosion simulations.

The results of the study clearly show the influence of variable fracture aperture on bentonite erosion behaviour and erosion rates (kg/a). Increasing fracture aperture standard deviation leads to increasing heterogeneous flow velocity distributions governing the erosion behaviour and erosion rates. Calculated steady state erosion rates are in the range of  $\sim 0.25$  kg/a down to  $\sim 0.014$  kg/a. The highest erosion rate is calculated for the highest mean flow velocity in conjunction with the highest standard deviation. The effect of aperture heterogeneity diminishes for the lowest flow velocities.

In summary, the results show the effect of fracture heterogeneity on bentonite erosion, especially for high to medium mean flow velocities combined with high to medium fracture heterogeneity under the model boundary conditions and model capabilities and limitations considered. An increase of up to  $\sim 83\%$  in erosion rate compared to the constant aperture case highlights the need to consider fracture aperture heterogeneity and its effect on the bentonite erosion in the assessment of the safety and evolution of a high-level nuclear waste repository.

### 1. Introduction

High level nuclear waste arises from different sources like e.g. nuclear power plants or reprocessing plants. Independent of the origin and type of high level waste it represents a threat to mankind due to its harmful radioactivity and chemo toxicity. Therefore, safe storage of the waste in deep geological repositories over long time scales is internationally agreed on. The KBS-3 concept in the Swedish safety case for the deep disposal of high-level nuclear waste is based on a multi-barrier

system to safely isolate the waste from the environment.<sup>1</sup> The first, so called technical barrier is represented by the waste form (e.g. vitrified waste or spent fuel) surrounded by a copper (or copper coated stainless steel) canister. The geotechnical barrier as the second building block of the multi-barrier concept is made of compacted bentonite encapsulating the waste canisters. The third and last barrier is the host rock itself in which the repository is built. In countries like e.g. Sweden, Finland, Russia, Korea, Czech Republic and China crystalline rock is favoured as host rock formation.

\* Corresponding author. Karlsruhe Institute of Technology (KIT) Institute for Nuclear Waste Disposal (INE), Hermann-von-Helmholtz-Platz 1, 76344, Eggenstein-Leopoldshafen, Germany.

E-mail address: [florian.huber@kit.edu](mailto:florian.huber@kit.edu) (F.M. Huber).

<https://doi.org/10.1016/j.ijrmms.2021.104742>

Received 15 March 2020; Received in revised form 25 February 2021; Accepted 25 March 2021

Available online 16 April 2021

1365-1609/© 2021 Elsevier Ltd. All rights reserved.

With respect to groundwater flow fractures and fracture networks are the only pathways within crystalline rock where advective flow can take place. Natural fractures are characterized by complex heterogeneous aperture distributions and complex overall geometries.<sup>2</sup> Numerous laboratory and numerical studies carried out in the last decades have shown the effect and importance of fracture geometry and aperture distributions on fracture flow fields.<sup>3–7</sup> One of the most pronounced fracture flow features is flow-channelling originating from geometrical heterogeneity and variability in fracture hydraulic conductivities as function of the fracture apertures. That is, areas of high flow velocities are localized next to low flow areas within the fracture. These flow gradients lead to complex patterns of fluid shear forces and hydrodynamic dispersion of solute and particles/colloids present in the seeping water.<sup>8</sup> One of the reference scenarios in the Swedish safety case is the intrusion of low mineralized glacial meltwater through fractures into the repository during interglacial periods.<sup>9</sup> The interaction of low mineralized waters with the bentonite barrier may lead to bentonite erosion and mass loss resulting in a worst case in the failure of the safety function of the geotechnical barrier. The interaction of different bentonites with both idealized aqueous systems (defined solutions) and natural systems (groundwater) has been studied extensively in the laboratory on a small scale<sup>10,11</sup> and recently also on the field scale.<sup>12</sup> Depending on the solution chemistry (especially in case of low divalent cation concentrations, divalent cation concentration below critical coagulation concentration (CCC)) and the influence of the smectite layer charge bentonite erosion can be quite pronounced.<sup>10,13</sup>

So far, only very few attempts have been made to develop mathematical or numerical models<sup>14</sup> to describe and forecast bentonite erosion. Probably the most sophisticated model available on bentonite erosion was presented by Neretnieks et al.<sup>15</sup> Applying this model, Moreno et al. presented model calculations on bentonite erosion in a parallel plate fracture<sup>14</sup> with a constant aperture of 1 mm and spatial fracture dimensions of at least 10 m × 5 m (model size depended on the imposed flow velocity). The simulations covered a range of mean velocities in the fracture of  $1 \times 10^{-5}$  m/s (315 m/a) down to  $1 \times 10^{-8}$  m/s (0.315 m/a). To achieve these velocities,<sup>14</sup> selected arbitrarily chosen constant hydraulic conductivities ( $1 \times 10^{-4}$  m/s to  $1 \times 10^{-7}$  m/s) assuming the validity of the Darcy law under these conditions were taken. Extending the work by Moreno<sup>14</sup> and Neretnieks<sup>15</sup> mentioned above, we used their model to investigate the potential impact of

fracture geometry (equivalent to flow field and mass transport heterogeneity) on bentonite erosion behaviour and erosion rates. The numerical studies conducted contribute to the mechanistic understanding of bentonite erosion relevant e.g. in the context of safety assessment of high level radioactive waste repositories.

## 2. Material and methods

### 2.1. Conceptual approach

The bentonite erosion model<sup>15</sup> was implemented in the software COMSOL Multiphysics (Multiphysics, 2015) and used by Moreno et al. in their simulations.<sup>14</sup> In the present study the identical model was applied implementing heterogeneous fracture aperture fields instead of the homogeneous aperture field previously used. The governing sets of equations for the description of the fluid flow (Darcy Law), bentonite expansion and erosion processes were therefore left untouched. The reader is referred to the papers by Moreno et al. Neretnieks et al. and Liu et al. for an extensive description of the theoretical basis and development of the bentonite erosion model.<sup>14–16</sup> The present paper only gives a brief overview of this model.

### 2.2. Model setup

In Fig. 1a, the model geometry, spatial dimensions and the boundary conditions for flow and mass transport are depicted. Water enters from the left side and leaves the domain only through the right border. At the top and at the bottom of the model both no flow and no flux conditions are applied on the model boundaries, respectively, except around the bentonite source which is allowed to swell and expand into the model domain. The diameter of the bentonite source is 1.75 m. On the left and right of the model domain pressure boundary conditions are applied to create a pressure gradient driving the water flow from left to right across the model domain. The pressure gradient was adjusted to obtain mean fracture flow velocities of  $1 \times 10^{-5}$  m/s,  $1 \times 10^{-6}$  m/s and  $1 \times 10^{-7}$  m/s, respectively. For computing the flow and bentonite erosion an unstructured triangular mesh is generated in COMSOL with a total of 13,362 elements and 6,839 nodes (Fig. 1b). Simulations were run until the erosion rate reached a steady state, i.e. a simulation time of at least 10 a, 100 a, and 1000 a for  $1 \times 10^{-5}$  m/s,  $1 \times 10^{-6}$  m/s and  $1 \times 10^{-7}$  m/

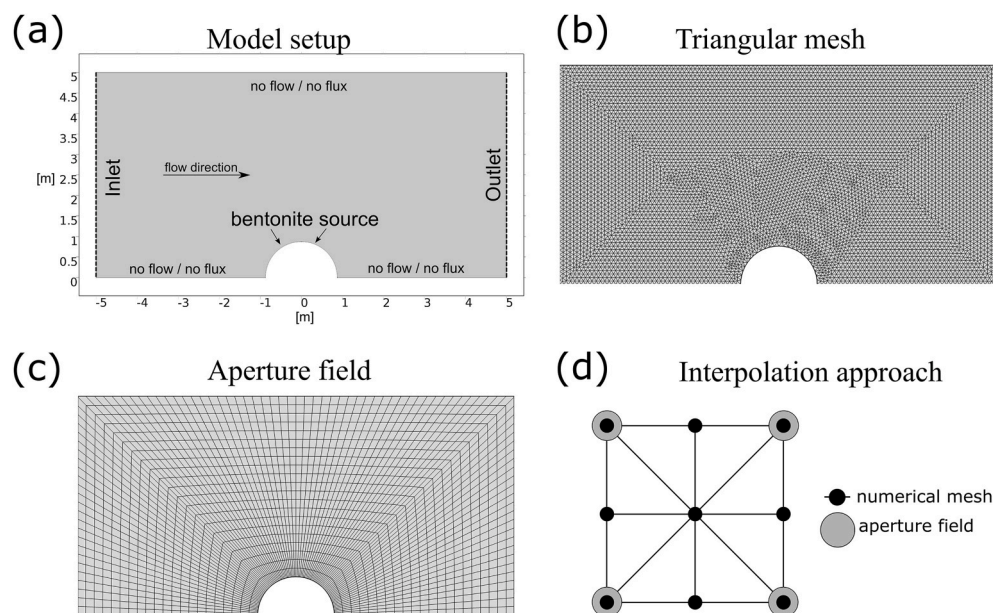


**Fig. 1.** (a) Model geometry, spatial dimensions and boundary conditions. (b) Numerical mesh used in COMSOL (c) Spatial distribution of the apertures (aperture field) (d) Generic scheme of the interpolation approach used between the triangular mesh and aperture field.

s, respectively. The bentonite erosion simulations conducted within this study were performed with the identical settings as in Ref. 14 except for the use of the variable aperture fields instead of the constant 1 mm aperture. That is, the background sodium concentration in the seepage water is 10 mM and the initial smectite volume fraction of the clay buffer is 40%. This is the considered smectite volume fraction in the clay at the mouth of the fracture, decreasing over tens of percent to some percents in the expanded bentonite gel in the fracture and down to fractions of percents in the very dilute suspension that we call sol.<sup>17</sup> For this sodium concentration a bentonite erosion is feasible since the critical coagulation concentration (CCC) has not been reached upon which a cohesive gel is forming inhibiting a colloid generation and erosion.<sup>14</sup>

### 2.3. Fracture aperture fields

Since data on detailed natural aperture distributions of field scale fractures are not available, synthetic randomized fracture aperture distributions were generated and used in the model simulations. From  $\mu$ -computed X-ray tomography ( $\mu$ CT) characterizations (resolution of 80  $\mu$ m and 32  $\mu$ m, respectively) of cm scale drill cores from Äspö, Sweden by e.g. Ref. 8, information on the natural fracture aperture distribution and fracture geometry/roughness is known. The measured aperture distributions follow normal or log-normal distributions (as both distributions give equally good fits, the normal distribution has been chosen in this study). Calculated mean apertures of two selected cores from Äspö, Sweden are 0.192 mm with a standard deviation (STD) of 0.064 mm and 0.451 mm with a STD of 0.14 mm, respectively. These two measurements display STDs in the range of  $\sim$ 30% of the mean aperture. Based on literature results, STDs of fracture apertures show a rather broad range from  $\sim$ 30% STD<sup>18</sup> up to more than 100% STD.<sup>19</sup> In the present study the fracture heterogeneity is modelled by varying the aperture field in a range of STDs from 10% up to 70% (STDs higher than 70% lead to numerical instabilities and were therefore discarded). That is, given a 1 mm mean aperture (as used by<sup>14</sup>), aperture fields with STDs of 0.1 mm (10%), 0.3 mm (30%), 0.5 mm (50%) and 0.7 mm (70%) are obtained in case of normal distributions. From the given distributions we calculate surface roughness  $\sigma_r$  and correlation length  $l_c$  according to the radial height-height correlation function:

$$H(\tau) = 2\sigma_r \left[ 1 - \exp\left(\frac{-\tau}{l_c}\right) \right]$$

In order to study both microscopic and macroscopic influences of the aperture field (and thus flow velocity distribution) on the bentonite erosion two different approaches to create the aperture fields have been employed. First, apertures have been randomly assigned to every node of the numerical triangular mesh according to normal distributions with a mean of 1 mm and STDs of 0.1 mm, 0.3 mm, 0.5 mm and 0.7 mm (corresponding to surface roughness  $\sigma_r$  of 0.1 mm, 0.3 mm, 0.5 mm and 0.7 mm). A regular distribution of apertures across the model domain was achieved by producing a quadratic mesh of the model domain within COMSOL (Fig. 1). The distribution (or resolution) of the mesh is not fully regular due to the model geometry with elements being smaller close to the cylindrical bentonite source. As an order of magnitude a resolution of 0.2 m on the borders was achieved yielding a correlation length between aperture node-values of  $\leq$ 0.2 m. We ignore the possibility of having asperities in our fractures which can be found in natural fractures, e.g. Ref. 8. The next step involved the assignment of a random aperture value of the normal distribution mentioned above on each node of the quadratic mesh. This aperture field was then used in COMSOL as input in an interpolation function (using the build-in capability of COMSOL). A simple linear interpolation function from the quadratic mesh to the numerical triangular mesh was chosen between the aperture values. In a second approach we employed a Monte-Carlo technique to create aperture distributions with the same mean of 1 mm and roughness of 0.1 mm, 0.3 mm, 0.5 mm and 0.7 mm, respectively. Aperture

node-values of every field are correlated by a correlation length of 1.75 m in the size range of the bentonite source. At least 10 different fields for each correlation length and roughness were generated to account for statistical variations. Especially for the high roughness ( $\sigma_r > 0.5$  mm) cases sometimes more than 10 different aperture fields were necessary to reach a converged result. Convergence was obtained when the difference between the steady state erosion rate became less than 3% of the mean erosion rate of all other fields for the same correlation length and roughness.

The triangular mesh has a finer resolution than the quadratic one (13,362 triangular elements compared to 2,219 aperture values of the quadratic mesh), especially around the bentonite source where the largest gradients are present. The choice of the triangular mesh size was driven by finding a compromise between simulation run time and numerical accuracy of the simulation. The triangular mesh resolution on the border is roughly 10 cm, i.e. a factor of 2 finer than for the aperture field. For the simulation of the flow and transport, the apertures are linearly interpolated onto the numerical grid nodes by COMSOL as mentioned above. A sketch is given in Fig. 1 to illustrate the interpolation approach.

Fig. 2 depicts plots of aperture fields for both correlation lengths and roughness of 0.1 mm and 0.7 mm, respectively. A superresolution factor of 1000 was chosen for visualization purposes. A clear difference can be seen between both the different correlation lengths of 0.2 m and 2 m and the roughness of 0.1 mm and 0.7 mm, respectively. As expected, the smaller correlation length aperture fields show a much higher peak density in contrast to the higher correlation length aperture fields. Moreover, the difference in roughness between 0.1 mm and 0.7 mm is clearly visible. A more quantitative way to compare the differences in the aperture fields is by plotting histograms for the two correlation lengths and the different roughnesses (Fig. 2e and f). As expected, for increasing STD or  $\sigma_r$  the distribution becomes increasingly broader.

### 2.4. Governing equations

A 2-d model is used in this work comprising (i) the flow of both water and bentonite, (ii) the bentonite expansion by a dynamic force balance model,<sup>16</sup> (iii) the advective and diffusive transport of sodium in the bentonite pore water and an empirical relation of the fluid viscosity (sodium concentration and bentonite volume fraction) based on experimental data. The before mentioned processes, briefly explained in the following subchapters, are strongly coupled and solved simultaneously within COMSOL. For an in-depth description of the governing equations the reader is kindly referred to the literature.<sup>14-16,20</sup>

### 2.5. Water and bentonite flow

Based on the aperture distributions hydraulic conductivity fields were calculated using the cubic law (Eq. 1) (Witherspoon et al., 1980):

$$K = \frac{\rho g}{12\mu} a^2 \quad (\text{Equation 1})$$

where  $K$  is the hydraulic conductivity [m/s],  $\rho$  is the density of water [kg/m<sup>3</sup>],  $g$  is the gravitational constant [m/s<sup>2</sup>],  $\mu$  is the dynamic viscosity [Pa·s] and  $a$  is the aperture [m]. The flow is solved subsequently by application of the Darcy equation within COMSOL (Eq. 2):

$$\vec{u} = \frac{T \cdot \vec{i}}{a} \quad (\text{Equation 2})$$

where  $u$  is the Darcy velocity [m/s],  $T$  is the transmissivity [m<sup>2</sup>/s],  $i$  is the hydraulic gradient over the domain [m/m] and  $a$  is the aperture [m].

The flow is strongly dependent on the fluid viscosity, that is, for high bentonite volume fraction the viscosity is high and the flow is thus very slow. Vice versa, for low bentonite volume fraction, the viscosity is low and the fluid flow more rapid. The transient behaviour of the fluid vis-

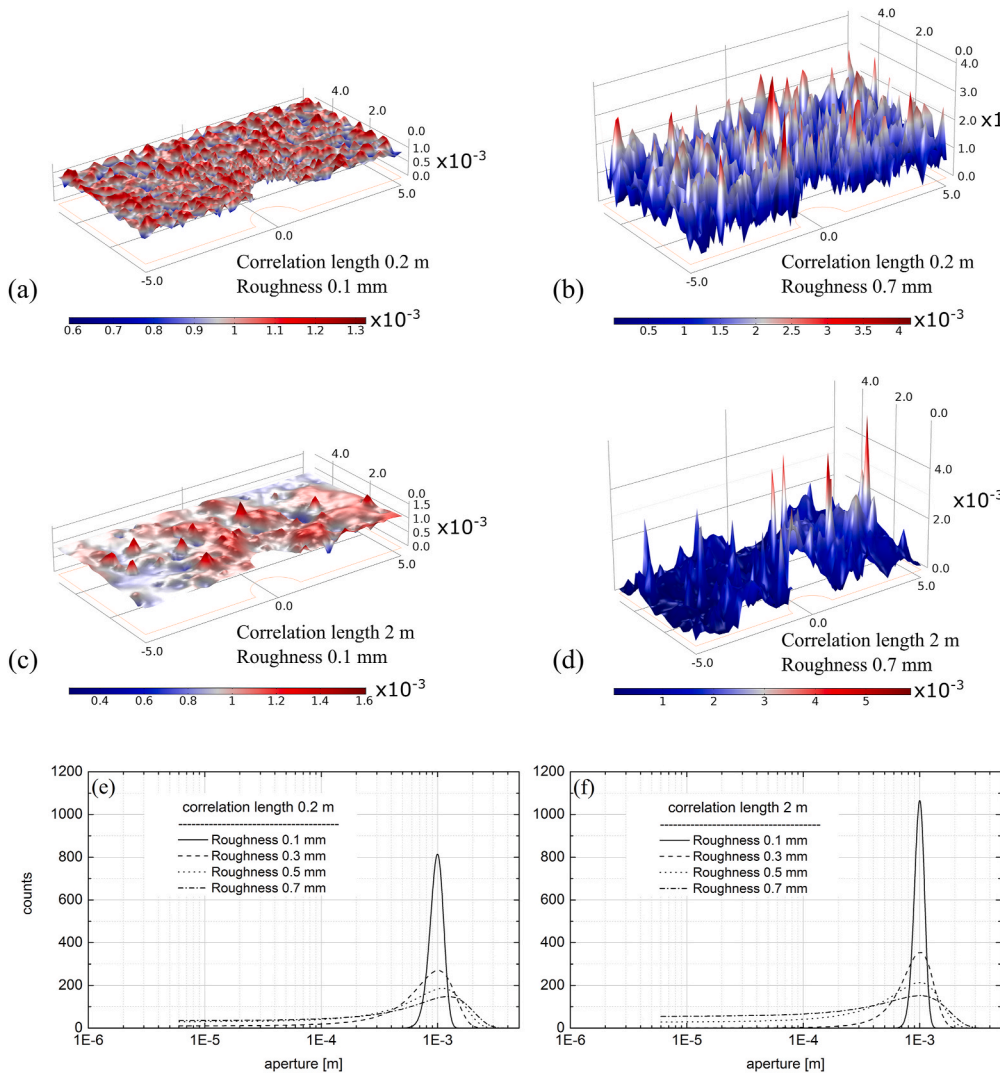


**Fig. 2.** (a & b) Graphical representation of aperture fields with a correlation length of 0.2 m and a roughness of 0.1 mm and 0.7 mm, respectively. (c & d) Graphical representation of two aperture fields with a correlation length of 2 m and a roughness of 0.1 mm and 0.7 mm, respectively (Please note the different color bar scales). (e & f) Histograms of aperture fields for both correlation lengths and all roughness (number of bins = 100). (For interpretation of the references to colour in this figure legend, the reader is referred to the Web version of this article.)

cosity is implemented in the Darcy equation. Fracture transmissivity  $T$  can be calculated by Equation (3):

$$T = T_w \frac{\eta_w}{\eta} \tag{Equation 3}$$

with  $\eta$  as fluid viscosity (N s/m<sup>2</sup>) and subscript w for water.

### 2.5.1. Advection-diffusion equation for sodium transport

The transport of Na in the fluid is modelled using the advection-diffusion equation which is given by Equation (4):

$$\frac{\partial c}{\partial t} = -\vec{u} \cdot \nabla c + \nabla \cdot (D \nabla c) \tag{Equation 4}$$

with cation concentration  $c$  (mol/m<sup>3</sup>), diffusion coefficient  $D$  (m<sup>2</sup>/s) and time  $t$  (s).

### 2.6. Bentonite expansion

A thorough overview of the bentonite (or smectite) expansion model is given by Liu et al.<sup>16</sup>. Only a summary is presented in the following. To describe the smectite mass balance an advection-diffusion-type equation is applied. It is given as (Equation (5)):

$$\frac{\partial \phi}{\partial t} = \vec{F}_s \cdot \nabla \left( \frac{\phi}{f} \right) - \vec{u} \cdot \nabla \phi + \nabla \cdot \left( \frac{\chi}{f} \nabla \phi \right) \tag{Equation 5}$$

with gravitational and buoyant force  $F_s$  (N), smectite volume fraction in the fluid  $\phi$  (–) and the energy sum of the particles  $\chi$  (J). The variable  $f$  accounts for the coupled movement of smectite particles into the fracture and an equivalent water volume moving in the opposite direction. It can be formulated as (Eq. 6):

$$f = f_{fr} / (1 - \phi) \tag{Equation 6}$$

where  $f_{fr}$  (N s/m) represents the friction coefficient between the smectite particles and the water. It can be written as (Eq. 7):

$$f_{fr} = 6\pi\eta_w r_{eq} + V_p k_0 \tau^2 a_p^2 \eta_w \frac{\phi}{(1 - \phi)^2} \tag{Equation 7}$$

where  $r_{eq}$  (m) is the equivalent radius of the non-spherical smectite particles, the pore shape factor  $k_0$  (–) and the flow channel tortuosity  $\tau$  ( $k_0 \tau^2$  is also known as Kozeny’s constant). The particles volume is given by  $V_p$  (m<sup>3</sup>) and the specific surface area per unit volume of particles is denoted as  $a_p$  (m<sup>2</sup>/m<sup>3</sup>).

The function  $\chi$  can be written as (Eq. 8):

$$\chi = k_B T + (h + \delta_p)^2 \left( \frac{\delta F_A}{\delta h} - \frac{\delta F_R}{\delta h} \right) \tag{Equation 8}$$

where  $k_B$  (J/K) represents the Boltzmann constant,  $T$  (K) the absolute temperature,  $h$  (m) the distance between the particles,  $\delta_p$  (m) the particle

thickness,  $F_A$  (N) van der Waal attractive forces and  $F_r$  (N) electrical repulsive forces, respectively. Partial derivatives of  $F_A$  and  $F_r$  are given in Liu et al. (2009).

The effective sodium diffusion coefficient in the fracture is a function of the smectite particles content and reduced compared to the diffusion coefficient in particle free water. Several correlations for the diffusion have been tested. Since only a weak sensitivity of the results depending on the correlation used have been obtained it was decided to use an Archie's law correlation for the diffusion.<sup>21</sup> It is written as (Eq. 9):

$$\frac{D}{D_0} = (1 - \phi)^{1.6} \tag{Equation 9}$$

with  $D_0 = 2 \times 10^{-9}$  m/s.

### 3. Results and discussion

#### 3.1. Fracture flow fields

Fig. 3 presents the flow velocity distributions (or flow fields) for the  $1 \times 10^{-6}$  m/s mean velocity for both correlation lengths and roughness of 0.1 mm and 0.7 mm. The flow field for the homogeneous case (Fig. 3 (left top)) shows two stagnation points with minimum flow velocities at

the front side and back side of the bentonite source. The highest flow velocities are found directly at the top of the bentonite source where the 2-d model has its smallest cross section accelerating the flow in this area.

At a larger distance from the bentonite source its influence decreases and the flow velocities tend to be more homogeneously distributed. The maximum velocity (under the given conditions of  $1 \times 10^{-6}$  m/s mean fracture velocity) is  $1.95 \times 10^{-5}$  m/s and the minimum velocity is  $7.77 \times 10^{-8}$  m/s, respectively. With increasing STD of the aperture distribution (reflecting higher fracture roughness or more complex fracture geometry, respectively), the flow field becomes more and more heterogeneous. In Fig. 3 (middle row) the flow field for a STD of 0.1 mm is shown. Compared to the homogeneous flow field (STD 0.0 mm), the flow velocities are distributed in a complex manner. Characteristically for flow in fractured media, areas of high flow velocities irregularly interchange with low flow areas leading to the phenomena of flow channelling. This can be clearly seen in Fig. 3 giving confidence in the approach chosen to simulate fracture flow fields. Whereas in case of 0.1 mm STD the homogeneous flow field pattern is still slightly visible, the flow field for a STD of 0.7 mm has changed dramatically. The flow field is now completely dominated by a large number of highly irregular and intersecting flow channels. Due to the higher spread of apertures with higher STD the range of flow velocities becomes broader. The gradients

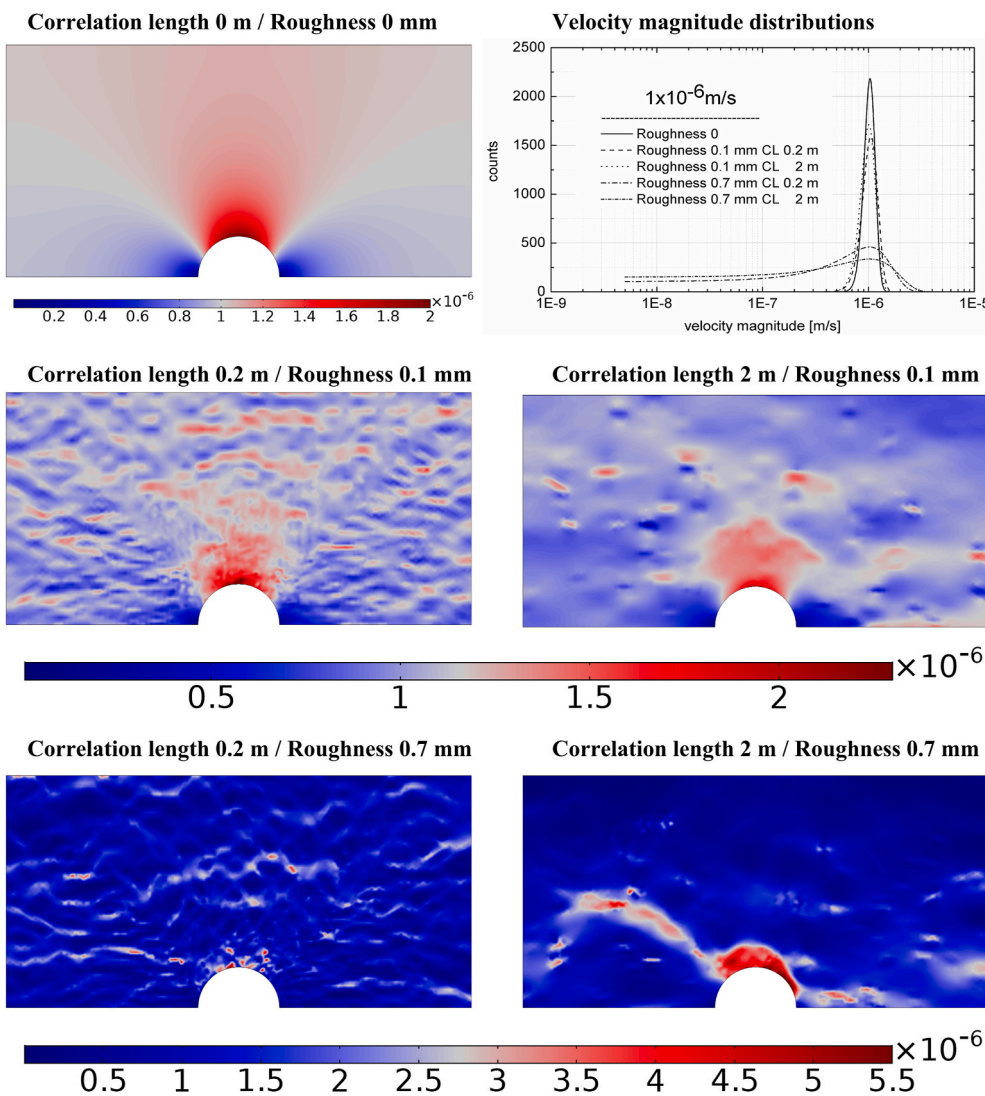


Fig. 3. Calculated velocity fields (Darcy velocity magnitude [m/s]) for a mean fracture velocity of  $1 \times 10^{-6}$  m/s. Note that the colour bars are different for visualization purposes. Blue colours represent low velocities, grey colours medium velocities and red colours high velocities, respectively. (For interpretation of the references to colour in this figure legend, the reader is referred to the Web version of this article.)

in flow velocities are much higher than for the lower STDs simulated spanning a range of more than 5 orders of magnitude. The maximum velocity increases with increasing STD from  $2.6 \times 10^{-5}$  m/s for STD 0.1 mm (range of velocities from  $9.11 \times 10^{-10}$  m/s up to  $2.66 \times 10^{-5}$  m/s) to  $3.87 \times 10^{-5}$  m/s for STD 0.7 mm (range of velocities from  $9.4 \times 10^{-11}$  m/s to  $3.87 \times 10^{-5}$  m/s; always given the same mean velocity within the whole domain).

With respect to the two different aperture correlation lengths of 2 m and 0.2 m, the flow fields show similar trends and features. Again the flow fields become much more complex due to the increasing STD showing the development of flow channelling with increasing roughness, though the sizes of the flow channels are completely different for both aperture correlation lengths. The CL of 2 m shows much bigger channels as the 0.2 m small CL. The bentonite expansion and erosion patterns for the homogeneous case and for STD 0.7 mm as the most heterogeneous case are very similar. In consequence, there are much less channels present than it is the case for the CL of 0.2 m. The influence of the different flow fields is presented in the following chapters.

### 3.2. Bentonite expansion and erosion

The effect of fracture heterogeneity on bentonite erosion was studied numerically for a range of mean fracture flow velocities ( $1 \times 10^{-5}$  m/s,  $1 \times 10^{-6}$  m/s,  $1 \times 10^{-7}$  m/s), fracture roughness (STD 0.1, 0.3, 0.5, and

0.7 mm) and two CL (0.2 m and 2 m). Due to the vast amount of data generated only selected results are shown in the following figures and plots.

#### 3.2.1. Effect of flow velocity

Fig. 4 depicts results of bentonite extrusion and erosion for a mean fracture flow velocity of  $1 \times 10^{-5}$  m/s. In these plots the bentonite volume fraction is shown (in greyish filled contour lines around the bentonite source) superimposed to the corresponding Darcy velocity fields. Due to the rather high mean velocity prevailing, the bentonite source expansion into the fracture is very much inhibited due to the high extent of erosion. This is already the case for the homogenous flow field where the highest flow velocities are in the direct vicinity of the bentonite source. The bentonite expands more on the lee side of the bentonite source with respect to the flow direction where slower flow velocities prevail. Here, the shear forces acting on the bentonite source are weaker than on the luv side. This behaviour is visible independent of the STD or CL and thus occurs for all cases studied. For decreasing flow velocities, the shear forces interacting with the bentonite decrease as well. By comparison of Figs. 4 and 5, this effect can be clearly seen. In case of a mean velocity of  $1 \times 10^{-6}$  m/s, the bentonite expansion is distinctively higher (Fig. 5). Again the expansion is much more pronounced on the lee side of the bentonite source. Due to the coupling of the flow velocity to the bentonite volume fraction (and therefore the

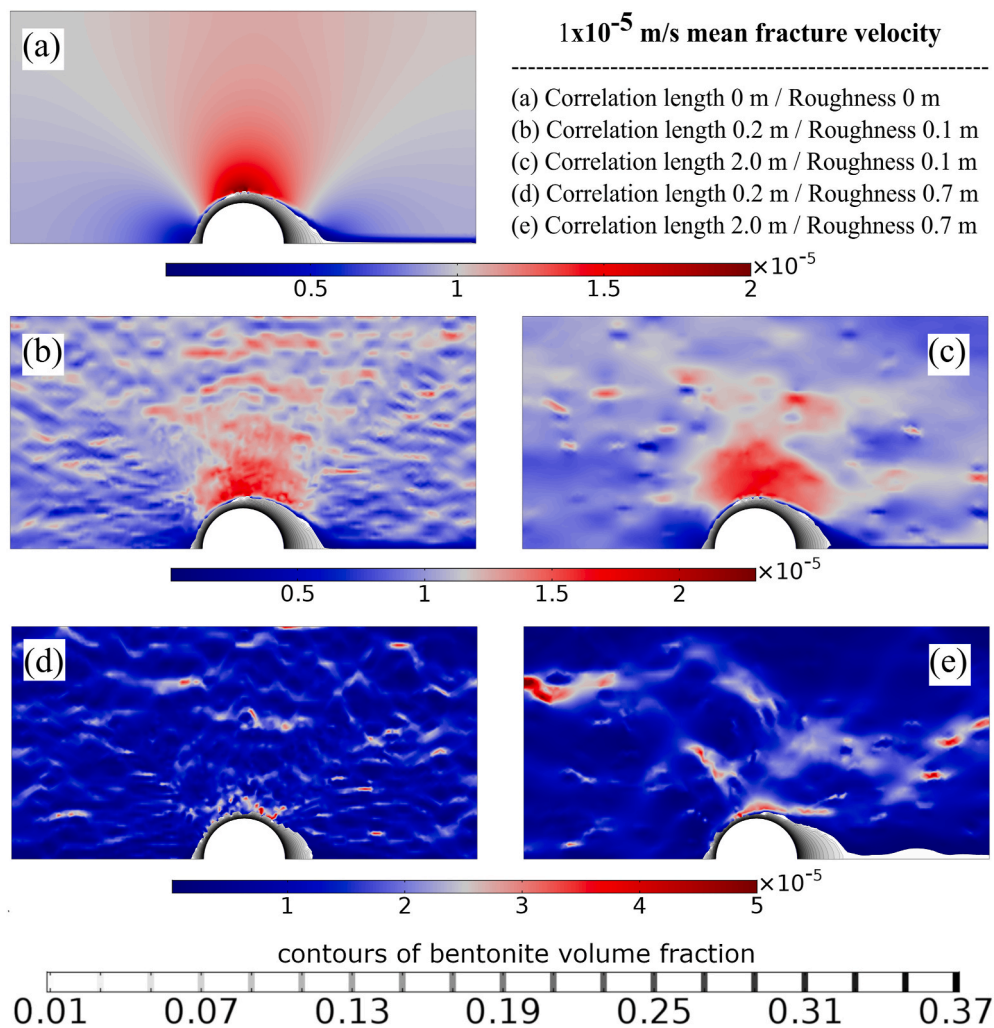


Fig. 4. Bentonite erosion patterns (greyish areas) for STDs of 0 mm (top), 0.1 mm (middle top), 0.1 mm (middle bottom) and 0.7 mm (bottom) for  $1 \times 10^{-5}$  m/s and both correlation lengths, respectively. Please note the different colour bars for each roughness. (For interpretation of the references to colour in this figure legend, the reader is referred to the Web version of this article.)

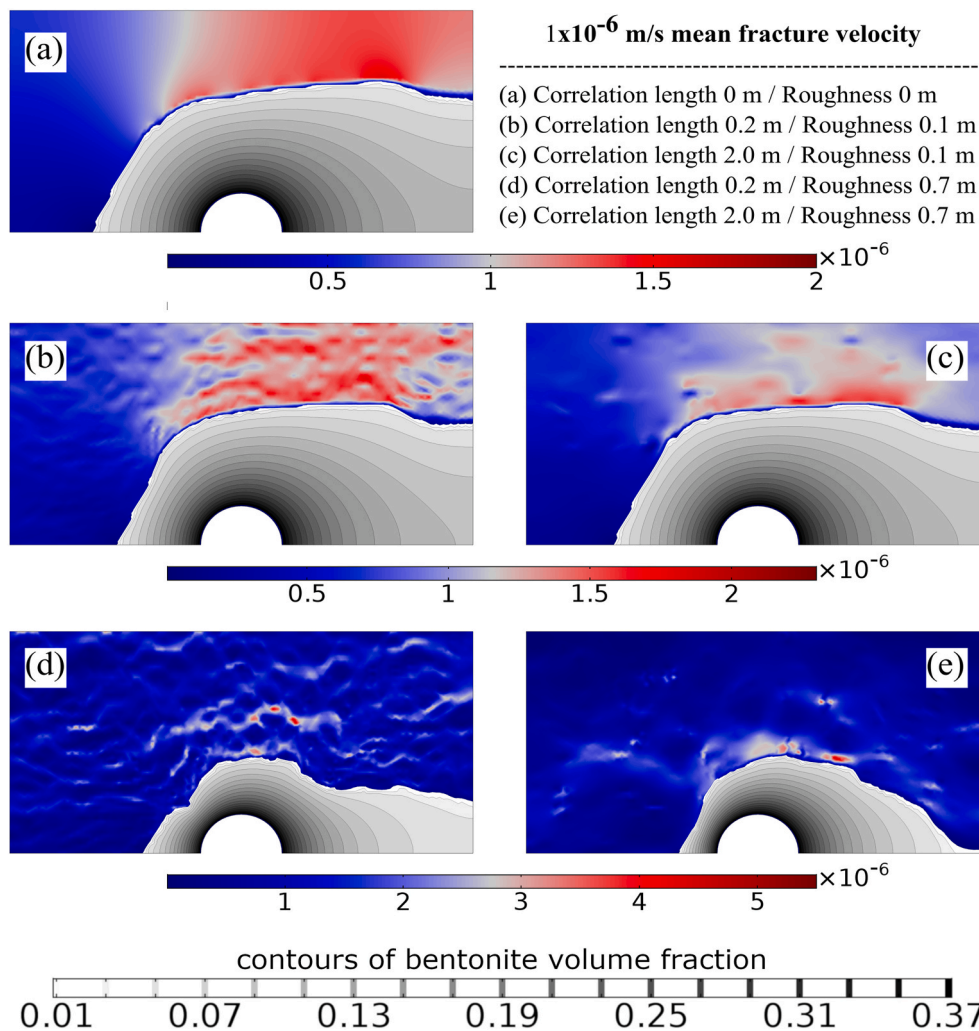


Fig. 5. Bentonite erosion patterns (greyish areas) for STDs of 0 mm (top), 0.1 mm (middle top), 0.1 mm (middle bottom) and 0.7 mm (bottom) for  $1 \times 10^{-6}$  m/s and both correlation lengths, respectively. Please note the different colorbars for each roughness.

water viscosity), the flow field is permanently changing during the transient bentonite expansion phase. This effect can be clearly seen when comparing the flow fields depicted in Fig. 3 (without bentonite expansion that is, the initial condition before any bentonite swelling and expansion has occurred) and Fig. 5 (steady state of the bentonite swelling and expansion for a mean flow velocity of  $1 \times 10^{-6}$  m/s). The bentonite displaces the flow leading to a decrease in cross sectional area of the flow domain. As a consequence, the flow velocities need to increase since the hydraulic pressure gradient over the whole domain is kept constant. Eventually, the volume fraction of the bentonite decreases to a level low enough to allow the bentonite to be eroded by the flow resulting in a steady state erosion process. Fig. 6 shows results for the lowest flow velocity ( $1 \times 10^{-7}$  m/s) examined. Due to the very weak shear forces at this velocity, the bentonite is able to swell and expand more symmetrically and to a much greater extent into the fracture as it was the case for higher flow velocities or shear forces, respectively.

### 3.2.2. Effect of fracture heterogeneity and correlation length

The flow field heterogeneity has an effect on the bentonite erosion behaviour as shown in both Figs. 4 and 5, respectively. Here, plots for both  $1 \times 10^{-5}$  m/s and  $1 \times 10^{-6}$  m/s mean velocity with STDs of 0 mm, 0.1 mm and 0.7 mm are depicted. The results are presented for a simulation time of 10 a, that is, until the erosion rate and flow have reached a steady state. Regarding  $1 \times 10^{-5}$  m/s mean velocity, only slight differences in the erosion patterns are observed among the

different CL and roughness. Generally speaking, there is only little bentonite extrusion into the fracture as already mentioned above. The expansion is more pronounced on the lee side of the flow behind the bentonite source where a flow shadow exists. In this area, the lowest shear forces occur allowing the maximum bentonite expansion.

The opposite holds for areas with highest flow velocities e.g. at the top of the bentonite source. Here, the bentonite cannot swell and expand freely due to the shear forces of the flow acting on the bentonite carrying away the bentonite by advection constantly. As presented and discussed by Moreno et al.<sup>14</sup> the bentonite volume fraction must be below  $\sim 0.001$  to possess a viscosity low enough to be transported away by the flow. The effect of fracture heterogeneity on the bentonite erosion behaviour is best observed in the case of  $1 \times 10^{-6}$  m/s mean velocity shown in Fig. 5. Under these conditions the bentonite is able to swell and expand to a bigger extent into the fracture as it was the case for  $1 \times 10^{-5}$  m/s mean velocity. With increasing heterogeneity, the expanded bentonite area starts to grow irregularly. This deformation can clearly be correlated to local flow gradients induced by the aperture distribution. Moreover, the swelling and expansion process is becoming more and more hindered since local flow velocity variations become more and more pronounced. In consequence, flow channelling is dominating the flow field for high STDs. Depending on the location of these flow channels the bentonite is heterogeneously eroded which can be seen e.g. in Fig. 5d.

With respect to the fracture aperture CL, no pronounced effect on

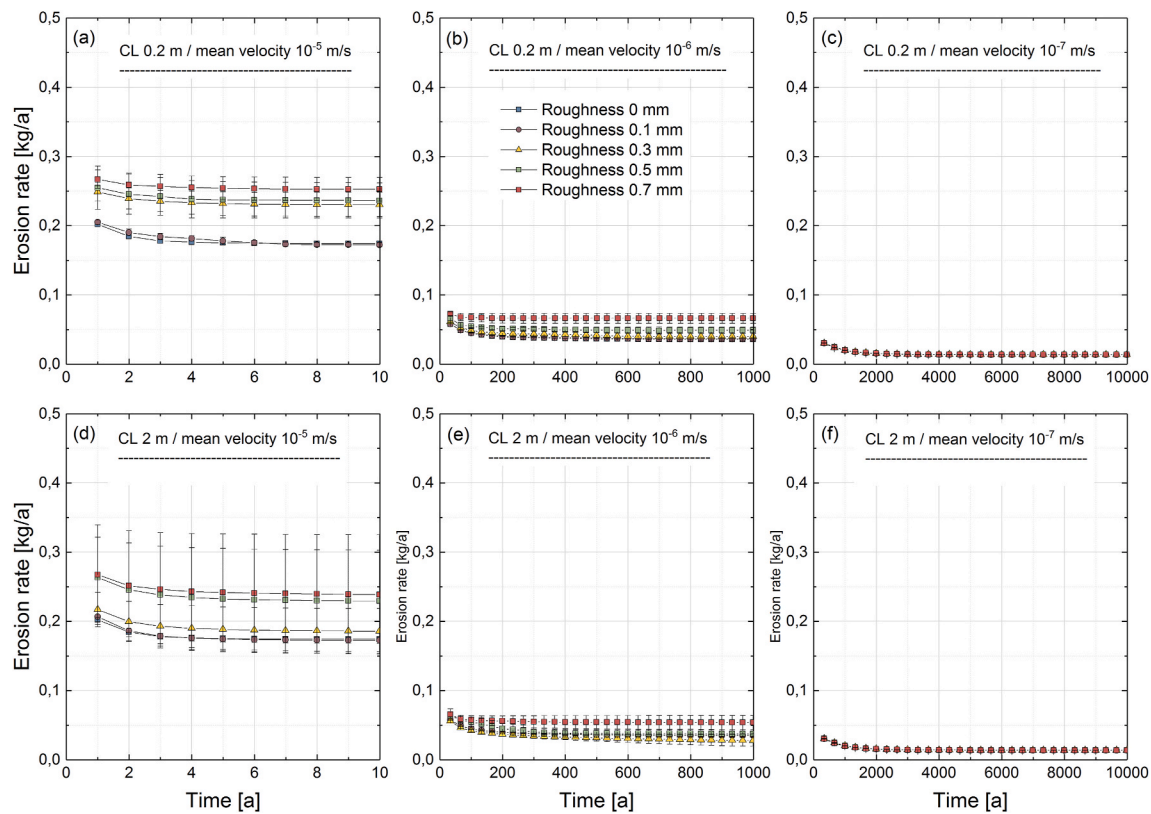


**Fig. 6.** Calculated bentonite erosion rates for all three mean velocities and both correlation lengths (CL) studied. Please note the different time scales for each velocity.

bentonite erosion is visible in Fig. 5. Here, both CL investigated (0.2 m and 2 m) are shown for STD 0.1 mm and 0.7 mm, respectively. The flow field is clearly different for both CL in terms of size and distribution of the flow channels present. For the higher CL the flow channels are much broader and less in number as already described in section 3.1. For the smaller STD of 0.1 mm, no difference can be seen for both CL used. A difference is visible for the higher STD of 0.7 between both CL. The expansion in Fig. 5d for 0.2 m CL is more pronounced on the lee side of the bentonite source in comparison to the 2 m CL expansion case. As mentioned above, the location and the size of the flow channels need to be considered when comparing the results for both CL. In Fig. 5e, a rather big flow channel on the lee side of the bentonite source might be responsible for the difference to the 0.2 m CL result. Since random aperture distributions are used in this work, the size and location of the flow channels vary between every model realization. A pronounced flow channel located far away from the bentonite source will consequently lead to a different expansion result due to a minor influence on the bentonite source.

By decreasing the mean flow velocity to  $1 \times 10^{-7}$  m/s the effect of the fracture heterogeneity is decreasing steadily (results not shown). The bentonite expansion and erosion patterns for the homogeneous case and for STD 0.7 mm as the most heterogeneous case are very similar. In both cases the bentonite expands completely into the fracture urging the flow velocities to become very low due to the high viscosity of the bentonite. That is, the flow shear forces are not high enough to exert a pronounced effect on the bentonite swelling and expansion process. For the heterogeneous case the expanded area is flattened very slightly at the top where the highest flow velocities are located verifying only minor heterogeneity effects on erosion.

### 3.2.3. Erosion rates

In conjunction to the rather qualitative results presented above, erosion rates have been calculated for all the different flow conditions

and STDs mentioned. The erosion rates are calculated as the bentonite flux (kg/a) over the bentonite source. The results are presented in Fig. 6 and Table 1. The erosion rates are shown for STDs of 0 mm, 0.1 mm, 0.3 mm, 0.5 mm, and 0.7 mm and for mean velocities of  $1 \times 10^{-5}$  m/s,  $1 \times 10^{-6}$  m/s, and  $1 \times 10^{-7}$  m/s, respectively.

**3.2.3.1. Correlation length 0.2 m.** In case of  $1 \times 10^{-5}$  m/s mean velocity, an erosion rate of 0.174 kg/a is obtained at the steady state reached after 10 a of simulation time for the homogeneous aperture field. No noticeable effect is visible for a STD of 0.1 mm compared to the homogeneous case. For a STD of 0.3 mm an increase in the erosion rate to 0.230 kg/a (+32%) was obtained. For the highest STD examined (0.7 mm), the erosion rate is further increased to a value of 0.252 kg/a (+45%).

With decreasing flow velocity, the differences in erosion rate is decreasing. For  $1 \times 10^{-6}$  m/s mean velocity, no difference in relation to the homogeneous case (0.0359 kg/a) is detectable for STD of 0.1 mm (+1.1%) and the differences for STD of 0.5 mm and 0.7 mm increases to +36% and +83%, respectively.

In the case of  $1 \times 10^{-7}$  m/s mean velocity no differences between the homogeneous case (0.0138 kg/a) are observed under steady state conditions after 10,000 a of simulation time for any STD considered. It is therefore safe to assume that erosion rates for a mean velocity below  $1 \times 10^{-7}$  m/s is also not affected by fracture heterogeneity.

**3.2.3.2. Correlation length 2 m.** For the  $1 \times 10^{-5}$  m/s mean velocity, the results for a CL of 2 m show much bigger error bars due to the bigger size of the flow channels and the importance of their spatial occurrence with respect to the bentonite source. The homogeneous case and the STD of 0.1 mm show equal erosion rates at steady state after 10 a simulation time. The erosion rate for the STD of 0.3 mm (0.186 kg/a) yields an increase of only 6.8%. Higher erosion rates are obtained for STDs of 0.5 mm and 0.7 mm, respectively. Here, an erosion rate increase of 31%

**Table 1**  
Calculated erosion rates (kg/a) as function of CL (m), STD (mm) and mean velocity (m/s).

Velocity (m/s)	CL 0.2 m					CL 2 m				
	STD 0.0 (mm)	STD 0.1 (mm)	STD 0.3 (mm)	STD 0.5 (mm)	STD 07 (mm)	STD 0.0 (mm)	STD 0.1 (mm)	STD 0.3 (mm)	STD 0.5 (mm)	STD 0.7 (mm)
$1 \times 10^{-5}$	0.1724	0.1724 ±	0.2304	0.2363	0.2526	0.1724	0.1726	0.1859	0.2293	0.2387
	<.001	.003	±.017	±.025	±.017	<.001	<.004	<.033	<.073	<.086
$1 \times 10^{-6}$	0.0359	0.0363	0.0399	0.0488	0.0662	0.0359	0.0351	0.0278	0.0377	0.0359
	<.001	±.002	±.005	±.006	±.007	<.001	<.002	<.008	<.005	<.010
$1 \times 10^{-7}$	0.0138	0.0138	0.0138	0.0138	0.0138	0.0138	0.0138	0.0138	0.0138	0.0138
	<.001	<.001	<.001	<.001	<.001	<.001	<.001	<.001	<.001	<.001

(0.5 mm STD; 0.229 kg/a) and 37% (0.7 mm STD; 0.238 kg/a) is obtained. It is important to notice that the values given are mean values of erosion rate. Regarding the big error bars extreme values of >0.3 kg/a (>72%) are possible.

Similar to the results of the CL of 0.2 m, no difference in erosion rate is obtained for the homogeneous case and the STD of 0.1 mm for a mean flow velocity of  $1 \times 10^{-6}$  m/s after 1,000 a simulation time. Moreover, the STD of 0.3 mm shows even a decrease in erosion rate as opposed to the CL of 0.2 m. An explanation might be referred to the statistical approach chosen where at least 10 different aperture fields were applied. As already mentioned above, the location of the flow channels to the bentonite source plays a decisive role for the bentonite expansion and thus erosion process. This results in a higher variability in erosion rates compared to the smaller CL of 0.2 m on the one hand, but also to contradirectional results within the same CL on the other hand. Nevertheless, this finding is a single occurrence in all simulation results obtained and does not undermine the general trend and results. A small increase of only 5% yields the result for the STD of 0.5 mm whereas the STD of 0.7 mm shows a strong increase of 50% following the expected general trend for the highest STD.

In line with the results for the Cl of 0.2 mm and  $1 \times 10^{-7}$  m/s mean velocity, no differences between the homogeneous case (0.0138 kg/a) are observed under steady state conditions after 10,000 a of simulation time for any STD considered. Again, no effect of fracture heterogeneity on erosion rate for a mean velocity below  $1 \times 10^{-7}$  m/s is expected.

#### 4. Conclusions

The effect of flow field heterogeneity on bentonite erosion has been studied by means of numerical simulations. For this, normal distributed random fracture aperture distributions with a mean aperture of 1 mm have been generated for (i) standard deviations of STD 0.1 mm, 0.3 mm, 0.5 mm, and 0.7 mm and (ii) aperture correlation lengths of 0.2 m and 2 m, respectively. A range of mean fracture flow velocities was covered in the study ( $1 \times 10^{-5}$  m/s,  $1 \times 10^{-6}$  m/s, and  $1 \times 10^{-7}$  m/s).

The results presented clearly verify the impact of fracture heterogeneity on bentonite erosion for mean velocities higher than  $\sim 1 \times 10^{-7}$  m/s ( $\sim 3.15$  m/a). Generally speaking, the heterogeneous aperture fields induce flow field gradients and typical fracture flow features like flow channelling. In consequence, locally varying shear forces lead to irregular bentonite erosion patterns. With increasing flow velocity and standard deviation, the effect on bentonite erosion increases causing higher erosion rates and spatially irregular erosion patterns.

In terms of safety assessment of a nuclear waste disposal in crystalline rock where bentonite is foreseen as backfill material (geotechnical barrier) around the copper/steel canisters, the results highlight the importance of flow heterogeneities on bentonite erosion. SKB considers the loss of 1,200 kg from originally 22,000 kg in one emplacement bore hole as a buffer failure criterion.<sup>22</sup> Taking the maximum modelled erosion rates of 0.252 kg/a in the case of  $1 \times 10^{-5}$  m/s mean velocity, 0.0359 kg/a for  $1 \times 10^{-6}$  m/s mean velocity and 0.0138 kg/a in the case of  $1 \times 10^{-7}$  m/s mean velocity the failure criteria is reached after 4, 800a, 33,400a or 87,000 years under these hydraulic conditions,

respectively. However, one has to consider the period until the next glacial inception, which depends on the cumulative carbon emissions within the next centuries. Calculations for the northern hemisphere based on CO<sub>2</sub> concentration evolution predicts in the absence of human perturbations no substantial ice build-up in another 50,000 years and for moderate anthropogenic cumulative CO<sub>2</sub> emissions of 1,000 to 1,500 gigatons of carbon the next glacial inception is not earlier predicted than in 100,000 years.<sup>23</sup> With respect to the very long time scales during which the repository might be exposed to quite drastic changes in hydrogeological conditions (e.g. high flow gradients following glacial periods), bentonite erosion and potential loss of barrier function is clearly a transient process which needs to be taken into consideration. The results of this study add an important aspect to the waste disposal safety assessment process and emphasize the implementation of heterogeneous bentonite erosion processes due to fracture aperture variability into sound predictions on the long-term stability of the geotechnical barrier.

#### Declaration of competing interest

The authors declare that they have no known competing financial interests or personal relationships that could have appeared to influence the work reported in this paper.

#### References

- Marty NCM, Fritz B, Clement A, Michau N. Modelling the long term alteration of the engineered bentonite barrier in an underground radioactive waste repository. *Appl Clay Sci.* 2010;47:82–90.
- Adler PM, Thovert J-F. *Fractures and Fracture Networks*. Dordrecht [u.a.: Kluwer; 1999.
- Detwiler RL, Rajaram H, Glass RJ. Solute transport in variable-aperture fractures: an investigation of the relative importance of Taylor dispersion and macrodispersion. *Water Resour Res.* 2000;36:1611–1625.
- Moreno L, Neretnieks I. Flow and nuclide transport in fractured media - the importance of the flow-wetted surface for radionuclide migration. *J Contam Hydrol.* 1993;13:49–71.
- Moreno L, Tsang C-F, Tsang Y, Neretnieks I. Some anomalous features of flow and solute transport arising from fracture aperture variability. *Water Resour Res.* 1990;26:2377–2391.
- Tsang CF, Neretnieks I. Flow channeling in heterogeneous fractured rocks. *Rev Geophys.* 1998;36:275–298.
- Tsang YW. The effect of tortuosity on fluid-flow through a single fracture. *Water Resour Res.* 1984;20:1209–1215.
- Huber F, Enzmann F, Wenka A, Bouby M, Dentz M, Schäfer T. Natural micro-scale heterogeneity induced solute and nanoparticle retardation in fractured crystalline rock. *J Contam Hydrol.* 2012;133:40–52.
- Neretnieks I, Moreno L. *Revisiting Bentonite Erosion Understanding and Modelling Based on the BELBaR Project Findings*. Stockholm, Sweden: SKB Svensk Kärnbränslehantering AG; 2018:52. Technical Report TR-17-12.
- Alonso U, Missana T, Fernandez AM, Garcia-Gutierrez M. Erosion behaviour of raw bentonites under compacted and confined conditions: Relevance of smectite content and clay/water interactions. *Appl Geochem.* 2018;94:11–20.
- Schäfer T, Huber F, et al. Nanoparticles and their influence on radionuclide mobility in deep geological formations. *Appl Geochem.* 2012;27:390–403.
- Nagra. In: Schlickefieder L, Lanyon GW, Kontar K, Blechschmidt I, eds. *Nagra, Wettingen (Switzerland). Grimsel test site - investigation phase VI «colloid formation and migration project: site instrumentation and initiation of the long-term in-situ test»*. 2015:139.

- 13 Eriksson R, Schatz T. Rheological properties of clay material at the solid/solution interface formed under quasi-free swelling conditions. *Appl Clay Sci.* 2015;108: 12–18.
- 14 Moreno L, Liu L, Neretnieks I. Erosion of sodium bentonite by flow and colloid diffusion. *Phys Chem Earth.* 2011;36:1600–1606. Parts A/B/C.
- 15 Neretnieks I, Liu L, Moreno L. *Mechanisms and Models for Bentonite Erosion.* Stockholm, Sweden: Svensk Kärnbränslehantering AB; 2009. SKB Technical report TR-09-35.
- 16 Liu L, Moreno L, Neretnieks I. A dynamic force balance model for colloidal expansion and its DLVO-based application. *Langmuir.* 2009;25:679–687.
- 17 Moreno L, Neretnieks I, Liu L. *Modelling of Erosion of Bentonite Gel by Gel/sol Flow.* Stockholm, Sweden: Svensk Kärnbränslehantering AB; 2010. SKB Technical Report 10-64.
- 18 Hakami E, Larsson E. Aperture measurements and flow experiments on a single natural fracture. *Int J Rock Mech Min Sci Geomech Abstr.* 1996;33:395–404.
- 19 Keller A. High resolution, non-destructive measurement and characterization of fracture apertures. *Int J Rock Mech Min Sci.* 1998;35:1037–1050.
- 20 Liu L, Moreno L, Neretnieks I. A novel approach to determine the critical coagulation concentration of a colloidal dispersion with plate-like particles. *Langmuir.* 2009;25: 688–697.
- 21 Archie GE. The electrical resistivity log as an aid in determining some reservoir characteristics. *Trans. AIME.* 1942;146:56–62.
- 22 SKB. *Long-term Safety for the Final Repository for Spent Nuclear Fuel at Forsmark, Main Report of the SR-Site Project* vol. I. Stockholm, Sweden: Svensk Kärnbränslehantering AB; 2011. SKB technical Report TR-11-1.
- 23 Ganopolski A, Winkelmann R, Schellnhuber HJ. Critical insolation - CO<sub>2</sub> relation for diagnosing past and future glacial inception. *Nature.* 2016;529:200–203.